

The He II lines in the Lyman series profiles of solar prominences

H. Ebadi^{1,2,3}, J.-C. Vial¹, A. Ajabshirizadeh^{2,3}

¹Institut d'Astrophysique Spatiale, Unité Mixte

CNRS-Université de Paris XI, Bat 121, 91405 Orsay, France

²Tabriz University, Faculty of Physics, Tabriz, Iran

³Research Institute for Astronomy and Astrophysics of Maragha,
55134-441 Maragha, Iran

Abstract. The hydrogen and helium lines are the most prominent lines in the solar prominences spectra. Observations with the SUMER spectrometer on board SOHO showed that there are weak lines in the blue wings of the Lyman series which affect their profiles. They were all identified as He II lines in the Lyman series wings, except for the La line whose profile was affected by the use of an attenuator. The He II lines are the even Balmer lines of the He II system, a set of lines that we complete with the odd ones. We characterize them by comparison with the blue wings of the Lyman series in order to improve the H Lyman series observations and modeling, on one hand and to provide He II lines observations for further combined H-He I-He II modeling, on the other hand.

key words: Sun; Prominences; Lyman lines; He II lines

1. Introduction

Labrosse et al. (2002) studied the hydrogen and helium lines emitted by a one-dimensional prominence model in magneto-hydrostatic equilibrium and in radial motion (Labrosse, Vial, and Gouttebroze, 2006; Labrosse, Vial, and Gouttebroze, 2008). The prominence slab consists of two parts: a cool core where the plasma is optically thick for some lines, and a prominence-to-corona transition region (PCTR) with a strong temperature gradient. The combination of H and He lines and continua systems allows for an in-depth diagnostic of these two basic components of the structure. Very optically thick lines provide information on the "surface" layers while optically thin lines and continua provide information on the volume from boundary to boundary. In this respect the Lyman series is of special interest because a single profile "scans" the line-of-sight structure and also because the lines of higher order are formed in the inner core of the prominence. In addition, helium lines provide more information either on the abundance of this element (which is not the issue here) or on the properties of both hotter (He singlet and He^+ lines) and colder (He triplet lines) material (Labrosse and Gouttebroze, 2001). Unfortunately, the resonance H and He lines are formed in very separate wavelength ranges (e.g. 304 Å for He II, 584 Å for He I and the Lyman series for H below 1216 Å), a fact which hampers simultaneous observations in H and He lines. It happens that close to each

© 2009 Springer Science + Business Media. Printed in the USA.

line of the Lyman series of H, some weak features appear in the quiet Sun which, after Feldman and Doschek (1991), Curdt et al. (2001) identified as He II lines and also in prominences (see e.g. Parenti, Vial, and Lemaire, 2004; Parenti, Vial, and Lemaire, 2005). And since they are formed in the wings of the Lyman lines, the relevant opacities are close to 1-10 (to be discussed later), contrary to the cores of the Lyman lines where the opacity can reach values as high as 10^6 for Ly α . Consequently, they offer a supplementary tool for diagnosing and modeling prominences, rather convenient as far as observations are concerned. Such "parasitic" lines (with references to the H Lyman lines) are well evident but a clear decomposition is not so easy because of the low signal-to-noise ratio and also because other lines are in competition, e.g. the D I lines. Actually, this is all the more interesting since the Deuterium abundance is an important quantity to be measured in the Universe, including the Sun (see e.g. Lubowich, 2003; Beckers, 1975). The helium and hydrogen lines are also useful diagnostic tools to study the active and eruptive prominence plasma.

In Section 2 we present the SUMER observations of Lyman lines and the full information about the data that we used. We refer to the SOHO images which are simultaneous to our data. This section also includes the data processing methods and software that we used through this work. The line identification methods are explained in Section 3 and our results in terms of "parasitic" and main H Lyman lines are presented in Section 4. Conclusions are drawn in Section 5.

2. Observations and data processing

SUMER is a high-resolution normal incidence spectrograph operating in the range 666-1610 Å (first order) and 333-805 Å (second order). The angular pixel size is 1''. The spectral pixel size depends slightly on the wavelength. Centroiding normally allows sub-pixel resolution. It can vary from about 45 mÅ pixel at 800 Å to about 41 mÅ/pixel at 1600 Å (see e.g. Wilhelm et al. 1995).

In order to identify the "parasitic" lines in the Lyman series, we used four different data sets which were obtained with SUMER. Their observation characteristics are presented in Table 1. The raw data have been initially processed applying the standard procedures for flatfield, deadtime and destretching correction which can be found in the Solar Software (SSW) database. We performed the radiometric calibration, so the specific intensity unit is $\text{W m}^{-2} \text{ sr}^{-1} \text{ Å}^{-1}$ through this analysis.

We integrated the lines over their profiles and plotted the intensities along the SUMER slit for the Lyman series from Ly α to Ly10 lines in Figure 2. As it is clear from this figure, the prominence region in Ly α is the pixel range

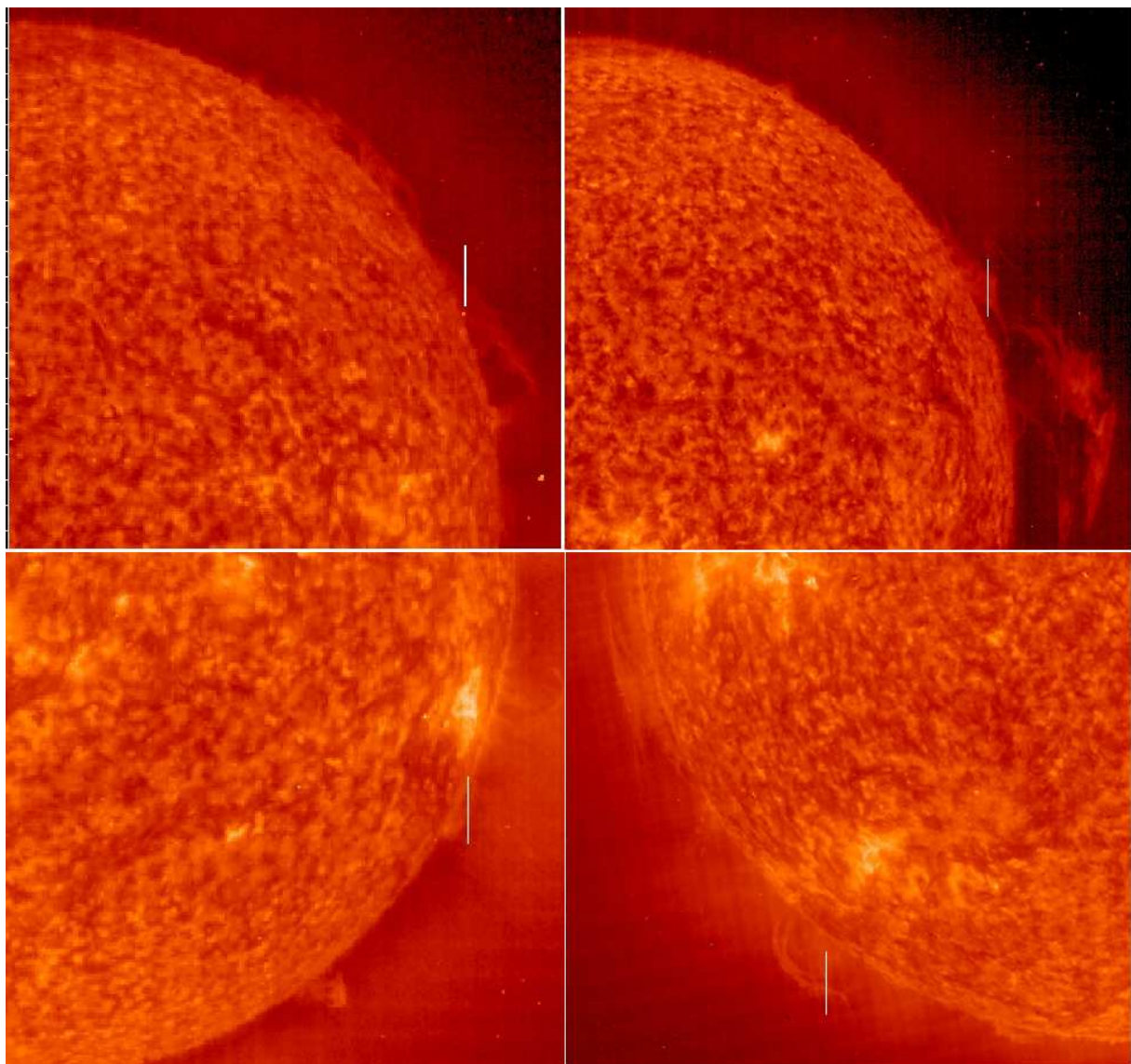


Figure 1. Images of the studied prominences in a) Ly α , b) Ly β , c) Ly γ , Ly4 and Ly5 and d) Ly6, Ly7, Ly8, Ly9 and Ly10 which were observed with SOHO/EIT in 304 Å. The SUMER slit is in the North-South direction.

Table I. Observation characteristics of the studied prominences.

Prominence	Lines observed	Date	Begin	End	Exposure times	Figure	Detector
1	Ly α	14 Jun 2004	20:15:42	20:21:52	370	1a	A
2	Ly β	7 Jun 2004	14:17:02	14:18:42	100	1b	A
3	Ly γ , Ly4 and Ly5	18 May 2001	11:47:15	11:48:53	98	1c	A
4	Ly6, Ly7, Ly8, Ly9 and Ly10	11 Jun 1998	11:02:51	11:04:31	100	1d	B

40-70, for Ly β it is from 37-119, for Ly γ , Ly4 and Ly5 it is from 65-85 and for Ly6, Ly7, Ly8, Ly9 and Ly10 is from 45-85.

3. Line identification

In order to identify the "parasitic" lines, we fitted Gaussian functions to such profiles with the least square method. The fitting yields the centers of the Lyman line and the weak line in its wing. The fitted function is as follows for reversed lines such as Ly α :

$$f(\lambda) = p_1 + p_2 e^{-2(\frac{\lambda-p_3}{p_4})^2} + p_5 e^{-2(\frac{\lambda-p_6}{p_7})^2} (1 - p_8 e^{-2(\frac{\lambda-p_6}{p_9})^2}) \quad (1)$$

and for the unreversed lines such as the lower Lyman series is assumed to be:

$$f(\lambda) = p_1 + p_2 e^{-2(\frac{\lambda-p_3}{p_4})^2} + p_5 e^{-2(\frac{\lambda-p_6}{p_7})^2} \quad (2)$$

The second term in the right-hand side of these equations is producing the "parasitic" lines and the third one corresponds to the Lyman lines. Typical results (in counts number, in order to evidence the statistics) are presented in the Figure 3 for Ly α and Ly β lines. It should be noted that the low counting rate for Ly α results from the use of the attenuator at the end of the detector. The attenuator is taken into account in the photometry.pro code.

In order to calculate the intensity ratios of the "parasitic" lines to proper Lyman lines, one can subtract their background continuum from the proper Lyman line one. We used this method for all of the mentioned Lyman lines and the results are presented in Table II. The identification of the "parasitic" lines as He II lines is relatively easy (see Table II) because of

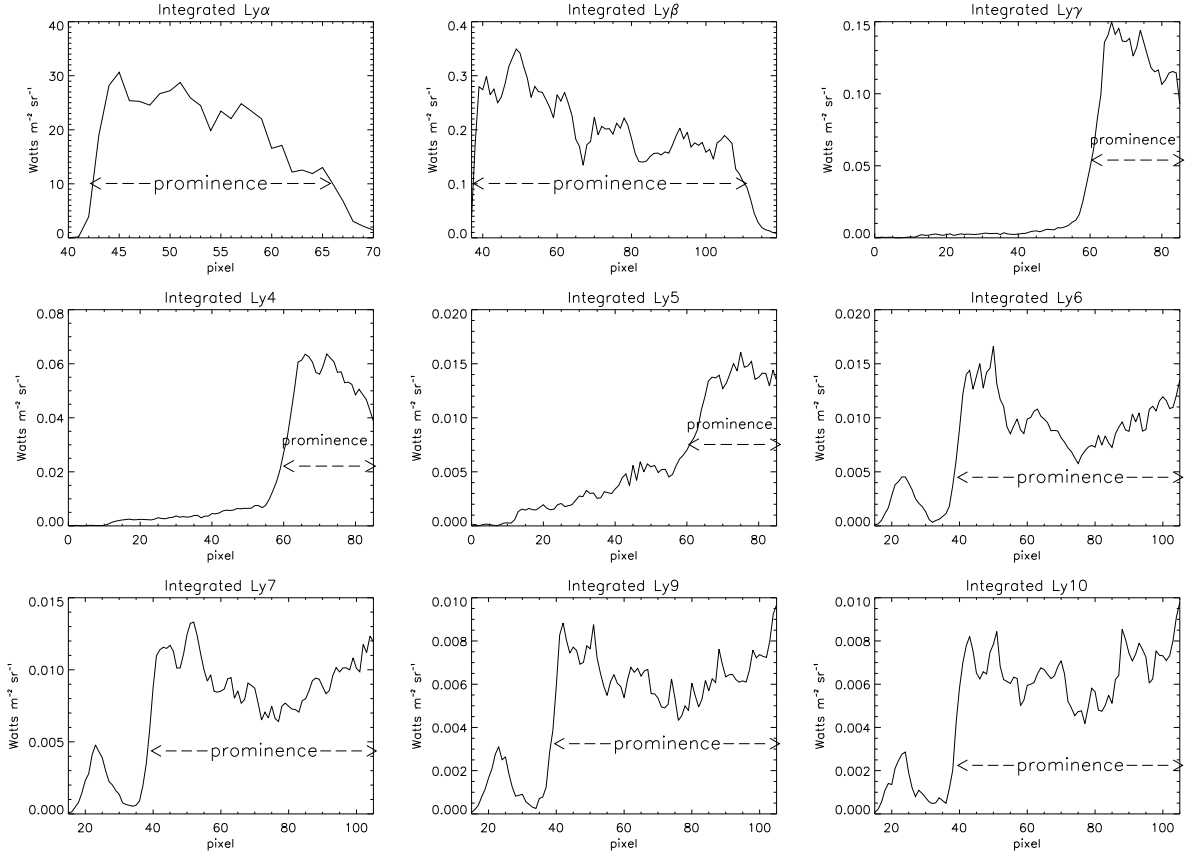


Figure 2. Cuts along the SUMER slit for the Lyman series lines and localization of the prominence (Ly8 was omitted).

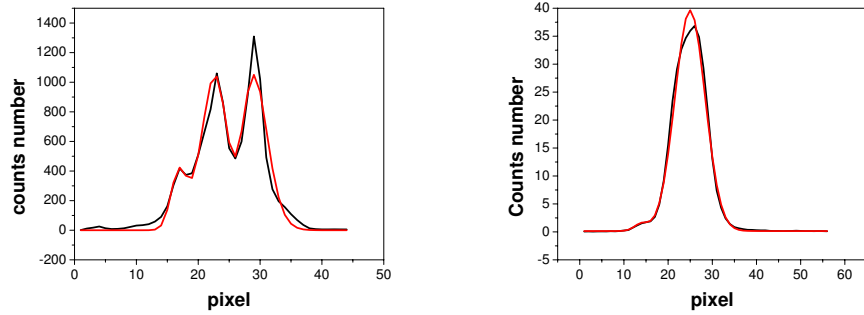


Figure 3. Typical Ly α (left) and Ly β (right) profiles, summed over all spatial pixels, (black lines) and fitted functions (red lines).

the close match between the wavelength of the observed peak in the Lyman line profile and the wavelength of the relevant He II line. (However, this assumes that the center of the H lines (whether the center of symmetry of the profile reversal or the gravity center of the whole profile) is located at the theoretical wavelength). This is true for all lines, except for the Ly α line where the observed "parasitic" line peak is at a wavelength separated from the (theoretical) He II line by about 100 mÅ, (more than twice the spectral pixel size). We checked that this separation is not affected by the method used for defining the H line center. We found that the three different criteria (position of the reversal dip, median of the reversal and median of the main profile) provide the same result within 0.2 pixel (9 mÅ). We tentatively explain this separation by the existence of a D line at 1215.339 Å, which, blended with the He II line, could provide the observed peak, since the separation between D and He II is 160 mÅ. However, one can question the effect of the attenuator (located close to the detector) on the line profile. Contrary to what has been observed by Heinzel et al. (2001) (see their Figure 6), the Ly α profile is rather smooth, with no apparent dip in both wings of the line, a fact confirmed by the good Gaussian fit. However, the impact of the attenuator upon the recorded profile being largely unknown, we prefer not to speculate on the observed emission/absorption feature and we discard the Ly α measurement from our set.

Table II. The "parasitic" lines wavelengths, transitions (Kelly 1987) and their intensity ratios to the neighboring Lyman lines (R) are presented .

$\lambda_{observed}$ (Å)	$\lambda_{abs.}$ (Å)	Line	Transition	R×100	$\frac{\Delta R}{R} \times 100$	Lyman line
1025.239	1025.241	He II	2p $^2P_{\frac{3}{2}}$ → 6d $^2D_{\frac{3}{2}}$	1.53	5	Ly β
972.1	972.083	He II	2p $^2P_{\frac{3}{2}}$ → 8d $^2D_{\frac{3}{2}}$	4.94	3	Ly γ
949.289	949.301	He II	2p $^2P_{\frac{3}{2}}$ → 10d $^2D_{\frac{3}{2}}$	16	3	Ly4
937.387	937.390	He II	2p $^2P_{\frac{3}{2}}$ → 12d $^2D_{\frac{5}{2}}$	9.73	5	Ly5
930.326	930.320	He II	2p $^2P_{\frac{3}{2}}$ → 14d $^2D_{\frac{5}{2}}$	5.32	3	Ly6
925.806	925.822	He II	2p $^2P_{\frac{3}{2}}$ → 16d $^2D_{\frac{5}{2}}$	4.15	4	Ly7
922.742	922.748	He II	2p $^2P_{\frac{3}{2}}$ → 18d $^2D_{\frac{5}{2}}$	1.56	7	Ly8
920.586	920.561	He II	2p $^2P_{\frac{3}{2}}$ → 20d $^2D_{\frac{5}{2}}$	4.16	5	Ly9
918.98	918.950	He II	2p $^2P_{\frac{3}{2}}$ → 22d $^2D_{\frac{5}{2}}$	1.63	8	Ly10

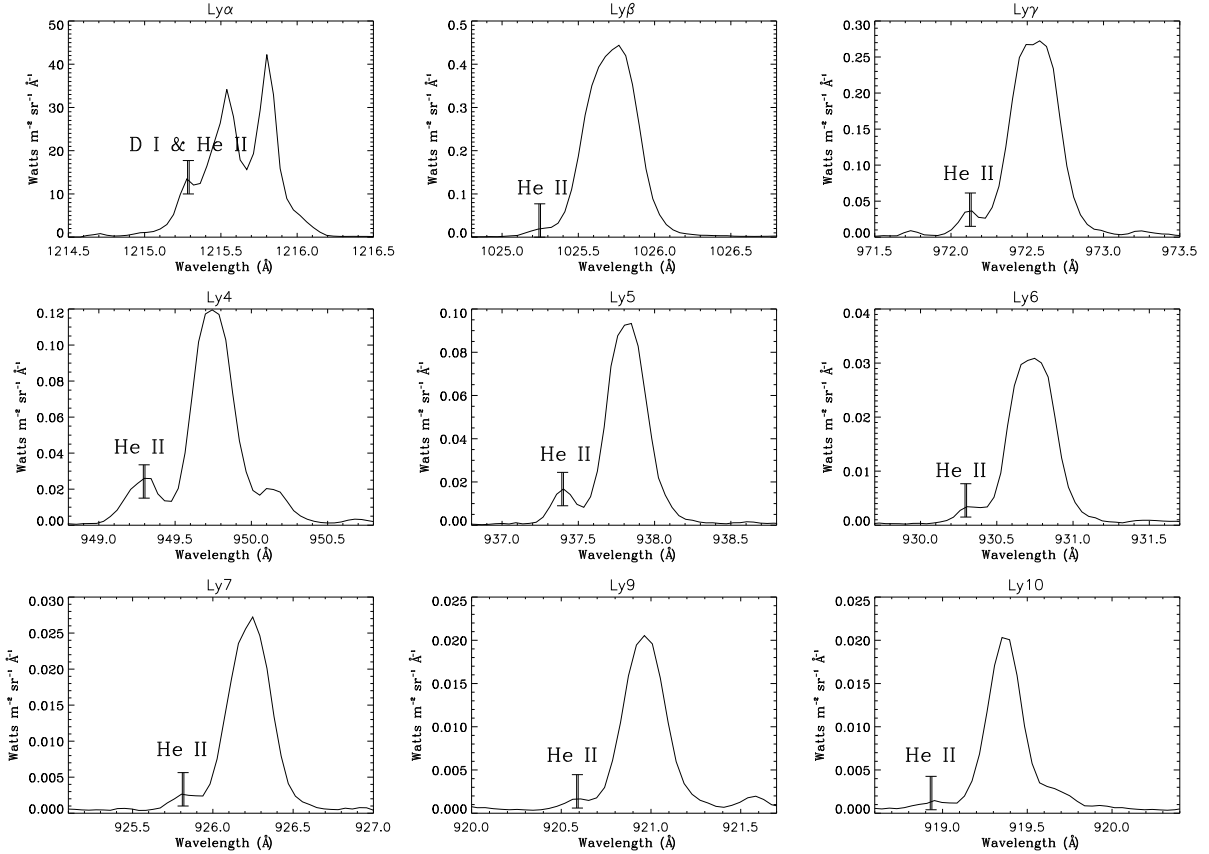


Figure 4. Profiles of Lyman line series and the He II and D I lines in the blue wings of H lines (Ly8 was omitted).

4. Discussion and conclusions

We presented the first identification of nine He II lines formed in the blue wings of the Lyman series in a solar prominence, as observed with SUMER/SOHO. Except for Ly α all other "parasitic" lines directly correspond to the even part of the Balmer series of He II where the common lower level is 2p 2P . This level (or more accurately, its three components) is the upper level of the resonance transition at 304 Å. Since the (even) Balmer lines appear in the strong Lyman profiles, there certainly is a strong radiative pumping by the Lyman photons from the lower 2p 2P level. It would be worth to check how this pumping affects the upper level of the 304 Å transition, and consequently its intensity.

Table III. Lines wavelengths of Balmer odd members of He II, transitions (Kelly 1987) and their intensity ratios to the mentioned neighboring even He II lines (R) are presented.

$\lambda_{observed}$ (Å)	$\lambda_{abs.}$ (Å)	Line	Transition	R	neighbor even He II line(Å)
1084.990	1084.975	He II	$2p\ ^2P_{\frac{3}{2}} \rightarrow 5d\ ^2D_{\frac{3}{2}}$	2.62	1025.239
992.382	992.391	He II	$2p\ ^2P_{\frac{3}{2}} \rightarrow 7d\ ^2D_{\frac{3}{2}}$	0.84	972.1
958.746	958.724	He II	$2p\ ^2P_{\frac{3}{2}} \rightarrow 9d\ ^2D_{\frac{3}{2}}$	0.30	949.289
942.457	942.510	He II	$2p\ ^2P_{\frac{3}{2}} \rightarrow 11d\ ^2D_{\frac{3}{2}}$	1.27	937.387
933.409	933.440	He II	$2p\ ^2P_{\frac{3}{2}} \rightarrow 13d\ ^2D_{\frac{3}{2}}$	1.54	930.326
927.822	927.860	He II	$2p\ ^2P_{\frac{3}{2}} \rightarrow 15d\ ^2D_{\frac{3}{2}}$	1.06	925.806

As for the L α "parasitic" line, future observations which provide the unmodulated Ly α profile are required to confirm this possible result.

Although the He II line profiles are rather narrow, we tried to identify their contributions to the Lyman profiles (see Section 3 and Table II). As far as integrated intensities are concerned, we found that their contributions vary from 1.5% (L β) up to 16% (Ly4) and down to 1.5% (L β and Ly10). The magnitude of these contributions is confirmed by the values of the odd Balmer lines detected in the spectrum. Table III shows that the intensity of odd lines is comparable (within a factor 3) to the intensity of the closest even lines. Let us note that the "abnormal" behavior of L δ was already noticed by Schmieder et al. (2007). We could not find any regular pattern. Are these ratios representative of He/H abundance? We do not think so since the He II and H lines are formed in different temperature regimes and consequently in different "layers" of the prominence. However, for opacity reasons, the photons in the He II lines and in this wavelength part of the H profiles are formed in the same region. One can ask whether the layer is optically thin at these wavelengths. Let us take the L β line: with a temperature of about 8000 K, a total opacity of 10^5 (see Gouttebroze, Heinzel, and Vial, 1993), the Voigt a-parameter is about 3×10^{-4} , which leads to a Voigt absorption at this wavelength of about 10^{-5} . This means that the (Hydrogen) opacity is of the order of 1 at this wavelength. The He II photons being formed in the external layers, they simply add up to the H photons formed deeper in the prominence. Consequently, it is impossible to derive any abundance information. We did not compute the various intensity ratios 2p-6d / 2p-4d, 2p-8d / 2p-4d, .. up to 2p-22d / 2p-4d in order to evaluate some Balmer decrement because measurements are not simultaneous or do not refer to

the same features. As far as He II lines widths are concerned, we found a rather wide range of values, with no systematic trend in the He II Balmer series. They tend to indicate either temperatures of about 30 000 K or a "microturbulence" up to 20 km s⁻¹ or any intermediate set of values.

As a conclusion, we think that it is worth further investigating the even Balmer He II lines located in the blue wing of the H Lyman series. More observations (if possible with a better spectral resolution) would allow to derive the profiles of these lines. Joint H and He II modeling (with a sufficient number of levels for He II) would lead to a better understanding of H and He II formation and better models when combined with observations.

Acknowledgments: SUMER is financially supported by DLR, CNES, NASA and the ESA PRODEX program (Swiss contribution). SOHO is a mission of international cooperation between ESA and NASA. We appreciate the ISSI support in the frame of the "Spectroscopy and Imaging of Quiescent and Eruptive Prominences from Space" Team. The authors sincerely thank the anonymous referee for pointing out important issues in the two versions of the paper. We thank R. Lallement for useful discussion about the D abundance.

References

- Beckers, J. M.: 1975, *Astrophysical Journal*, **195**, L43.
 Curdt, W., Brekke, P., Feldman, U., Wilhelm, K., Dwivedi, B.-N., Schühle, U., Lemaire, P.: 2001, *Astron. Astrophys.*, **375**, 591.
 Feldman, U., Doschek, G. A.: 1991, *Astrophys. J. Suppl. Ser.*, **75**, 925.
 Gouttebroze, P., Heinzel, P., Vial, J.-C.: 1993, *Astron. Astrophys. Suppl. Ser.*, **99**, 513.
 Heinzel, P., Schmieder, B., Vial, J.-C., Kotrc, P.: 2001, *Astron. Astrophys.* **370**, 281.
 Kelly, R. L.: 1987, Atomic and ionic spectrum lines below 2000 Angstroms. Hydrogen through Krypton (New York: American Institute of physics (AIP), American chemical Society and the National Bureau of Standards, 1987).
 Labrosse, N., Gouttebroze, P.: 2001, *Astron. Astrophys.*, **380**, 323.
 Labrosse, N., Gouttebroze, P., Heinzel, P., Vial, J.-C.: 2002, *ESA SP-506*, **451**.
 Labrosse, N., Vial, J.-C., Gouttebroze, P.: 2006, Solar Active Regions and 3D Magnetic Structure, 26th meeting of the IAU, Joint Discussion 3, JD03, 47.
 Labrosse, N., Vial, J.-C., Gouttebroze, P.: 2008, *Ann. Geophys.*, **26**, 2961.
 Lubowich, D.A.: 2003, *Nuclear Physics*, **A718**, 395.
 Parenti, S., Vial, J.-C., Lemaire, P.: 2004, *Solar Phys.*, **220**, 61.
 Parenti, S., Vial, J.-C., Lemaire, P.: 2005, *Astron. Astrophys.*, **443**, 679.
 Schmieder, B., Gunár, S., Heinzel, P., Anzer, U.: 2007, *Solar Phys.* **241**, 53.
 Wilhelm, K., Curdt, W., Marsch, E., Schühle, U., Lemaire, P., Gabriel, A., Vial, J.-C., Grewing, M., Huber, M. C. E., Jordan, S. D., 6 coauthors: 1995, *Solar Phys.*, **162**, 189.

